Supporting Information for

Robust Calix[4]arene-Polyethyleneimine Coated Iron Oxide Nanoparticles for Enhanced Recovery of Gold and Platinum Chloride Complexes

Carlos Moya,[1-3] Natacha Brion,[4] Ludovic Troian-Gautier,[5-7] Ivan Jabin,[7] Gilles Bruylants[1*]

[1] Engineering of Molecular NanoSystems, Ecole polytechnique de Bruxelles, Université libre de Bruxelles, Brussels 1050, Belgium

[2] Departament de Física de la Matèria Condensada, Universitat de Barcelona, Martí i Franquès 1, 08028 Barcelona, Spain

[3] Institut de Nanociència i Nanotecnologia (IN2UB), Universitat de Barcelona, 08028 Barcelona, Spain

[4] Analytical and Environmental Geochemistry (AMGC), Vrije Universiteit Brussel, Pleinlaan 2, 1050 Brussels, Belgium

[5] Université catholique de Louvain (UCLouvain), Institut de la Matière Condensée et des Nanosciences (IMCN), Molecular Chemistry, Materials and Catalysis (MOST), Place Louis Pasteur 1, bte L4.01.02, 1348 Louvain-la-Neuve, Belgium

[6] Wel Research Institute, Avenue Pasteur 6, 1300 Wavre, Belgium

[7] Laboratoire de Chimie Organique, Université libre de Bruxelles, Avenue F.D. Roosevelt, 50 B-1050 Brussels, Belgium

***Corresponding author:** gilles.bruylants@ulb.be

Table of contents

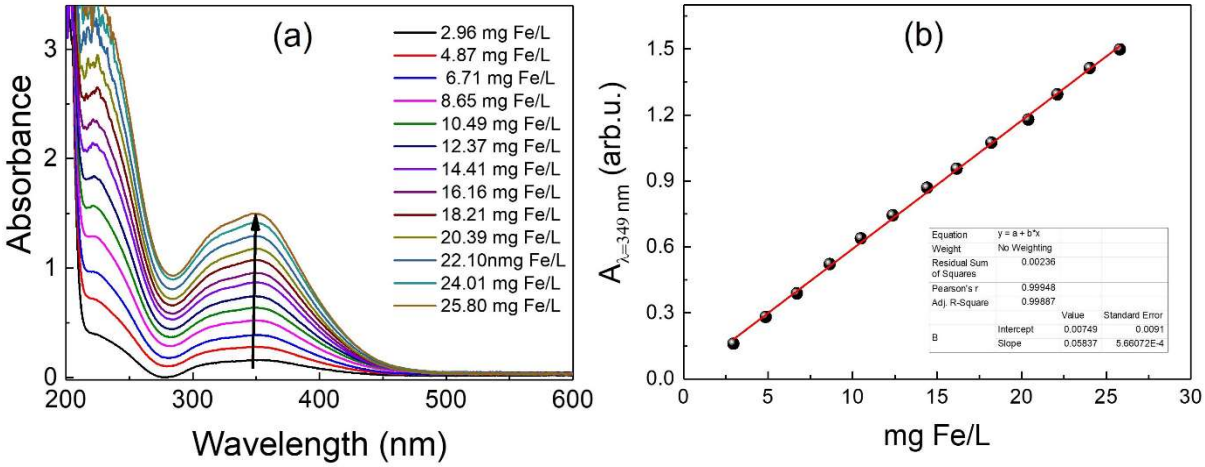

Figure S1. Calibration curve employed to quantify the Fe in the IONPs by the UV-vis protocol.[1] (a) Fe standard curves ranging from 200 to 800nm for [HCl]=5M employing $FeCl_3$ as the Fe source. (b) The calibration curve was obtained from the Fe standard curves with an R^2 of 0.99954.

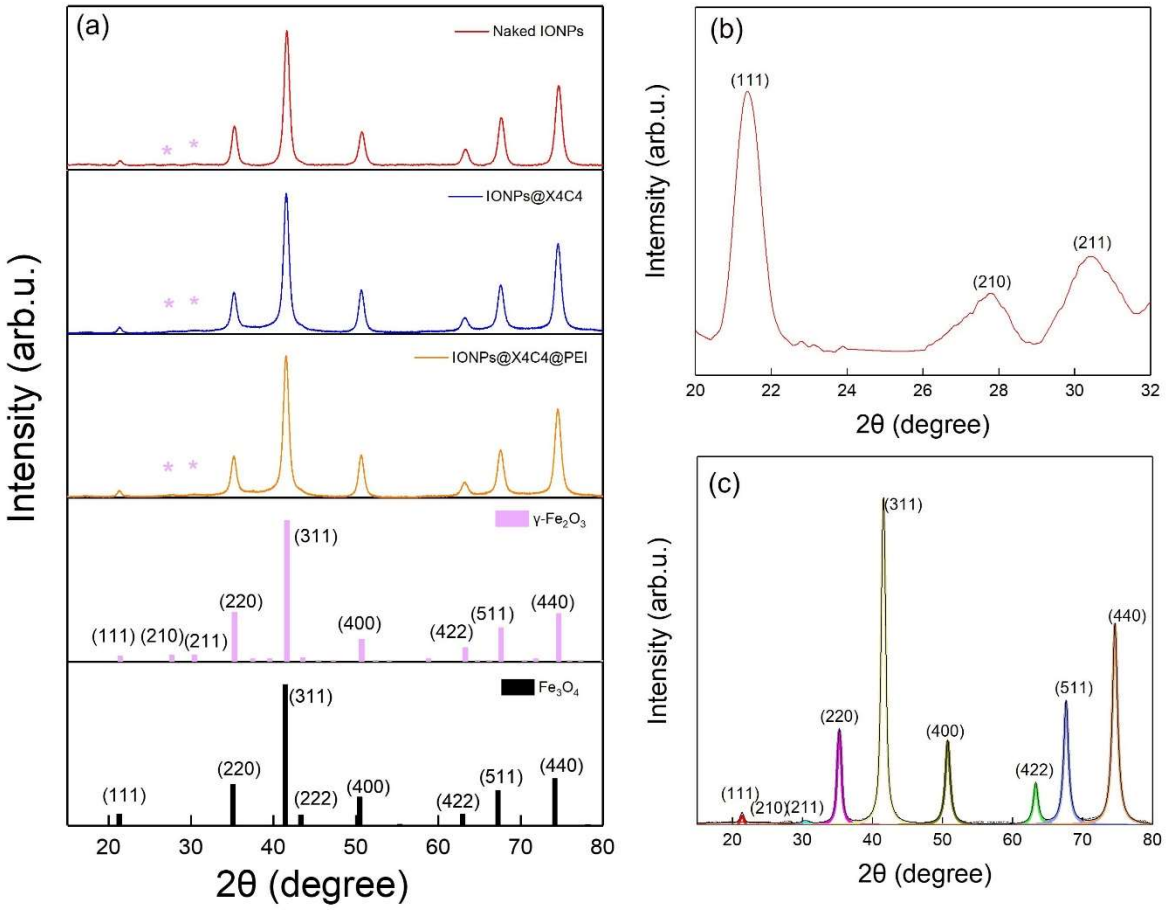

Figure S2. (a) XRD spectra from 15º to 80º for naked IONPs, IONPs@X4C4, and IONPs@X4C4@PEI, shown alongside reference patterns for the γ-Fe_2O_3 (ICSD: 00-039-1346) and Fe_3O_4 (ICSD: 01-089-3854) phases. (b) Zoomed-in section of the XRD spectrum for the naked IONPs, highlighting the peaks corresponding to the (111), (210), and (211) planes. (c) Voigt fitting of the XRD data from 15º to 80º for the naked IONPs sample.

Table S1. Detailed comparison of XRD data for (a) naked IONPs, (b) IONPs@X4C4, and (c) IONPs@X4C4@PEI. Columns from left to right show the experimental 2θ values for each sample, the assigned family of planes, the corresponding 2θ values from γ-Fe_2O_3 (ICSD: 00-039-1346), Fe_3O_4 (ICSD: 01-089-3854), the absolute differences for $|2\theta_{exp} - 2\theta_{\gamma-Fe_2O_3}|$ and for $|2\theta_{exp} - 2\theta_{Fe_3O_4}|$, the crystal size determined for each family of planes(D_{XRD}), and the lattice constat (a) assuming Face-Centered Cubic (FCC) structure.

(a)

2θ experimentals (Naked IONPs)	Assigned family of planes	2θ γ-Fe_2O_3 (ICSD: 00-039-1346)	2θ Fe_3O_4 (ICSD: 01-089-3854)	$\lvert 2\theta_{exp}$ - 2θγ-$Fe_2O_3\rvert$	$\lvert 2\theta_{exp}$ - 2θ$Fe_3O_4\rvert$	D_{XRD} (Å)	a=b=c (Å)
21.40	111	21.38	21.27	0.02	0.13	135.00	8.34
27.74	210	27.68	---	0.06	---	---	8.34
30.34	211	30.41	---	0.07	---	---	8.37
35.27	220	35.27	35.09	0.01	0.19	123.64	8.35
41.62	311	41.62	41.40	0.00	0.22	115.43	8.35
50.75	400	50.70	50.46	0.04	0.28	114.71	8.35
63.32	422	63.31	62.94	0.01	0.38	128.03	8.35
67.66	511	67.63	67.25	0.03	0.42	116.43	8.35
74.63	440	74.62	74.15	0.01	0.48	111.86	8.35

(b)

2θ experimentals (IONPs@X4C4)	Assigned family of planes	2θ γ-Fe_2O_3 (ICSD: 00-039-1346)	2θ Fe_3O_4 (ICSD: 01-089-3854)	$\lvert 2\theta_{exp}$ - 2θγ-$Fe_2O_3\rvert$	$\lvert 2\theta_{exp}$ - 2θ$Fe_3O_4\rvert$	D_{XRD} (Å)	a=b=c (Å)
21.27	111	21.38	21.27	0.11	0	124	8.40
27.82	210	27.68	---	0.14	---	---	8.32
30.54	211	30.41	---	0.13	---	---	8.32
35.22	220	35.27	35.09	0.04	0.14	109	8.36
41.56	311	41.62	41.40	0.07	0.16	110	8.36
50.69	400	50.70	50.46	0.01	0.23	133	8.36
63.60	422	63.31	62.94	0.29	0.66	121	8.32
67.60	511	67.63	67.25	0.03	0.35	119	8.36
74.56	440	74.62	74.15	0.06	0.41	119	8.35

(c)

2θ experimentals (IONPs@X4C4@PEI)	Assigned family of planes	2θ γ-Fe_2O_3 (ICSD: 00-039-1346)	2θ Fe_3O_4 (ICSD: 01-089-3854)	$\lvert 2\theta_{exp}$ - 2θγ-$Fe_2O_3\rvert$	$\lvert 2\theta_{exp}$ - 2θ$Fe_3O_4\rvert$	D_{XRD} (Å)	a=b=c (Å)
21.26	111	21.38	21.27	0.12	0.01	145	8.40
27.67	210	27.68	---	0	---	---	8.36
30.36	211	30.41	---	0.05	---	---	8.37
35.28	220	35.27	35.09	0.01	0.19	118	8.35
41.47	311	41.62	41.40	0.15	0.07	119	8.38
50.89	400	50.70	50.46	0.19	0.43	128	8.33
63.57	422	63.31	62.94	0.26	0.63	130	8.32
67.82	511	67.63	67.25	0.19	0.58	123	8.33
74.92	440	74.62	74.15	0.30	0.77	137	8.32

Table S2. Summary of D_{XRD}, a, and their corresponding standard deviations for the naked IONPs, IONPs@X4C4, and IONPs@X4C4@PEI samples, derived from the average values presented in Table 1.These results are compared with reference data for γ-Fe_2O_3 (ICSD: 00-039-1346) and Fe_3O_4 (ICSD: 01-089-3854).

determined average a(Å)	Standard deviation (Å)	a γ-Fe_2O_3 (00-039-1346(Å)	a Fe_3O_4 (01-089-3854 (Å)
8.35	0.01	8.35	8.39
8.35	0.02	8.35	8.39
8.35	0.03	8.35	8.39

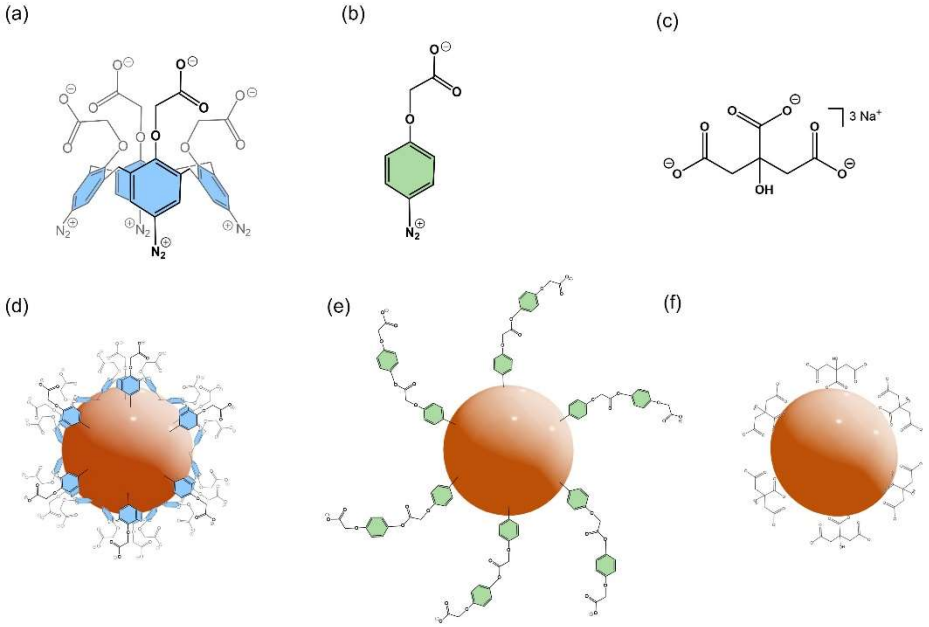

Figure S3. Molecular representation of the organic agents utilized to functionalize the IONPs. (a) and (b) Show the diazonium salts of X4C4 and XC under their acidic form, respectively. (c) Trisodium citrate. Representation of the functionalized IONPs. (d) IONPs@X4C4, (e) IONPs@XC, and (f) IONPs@Cit.

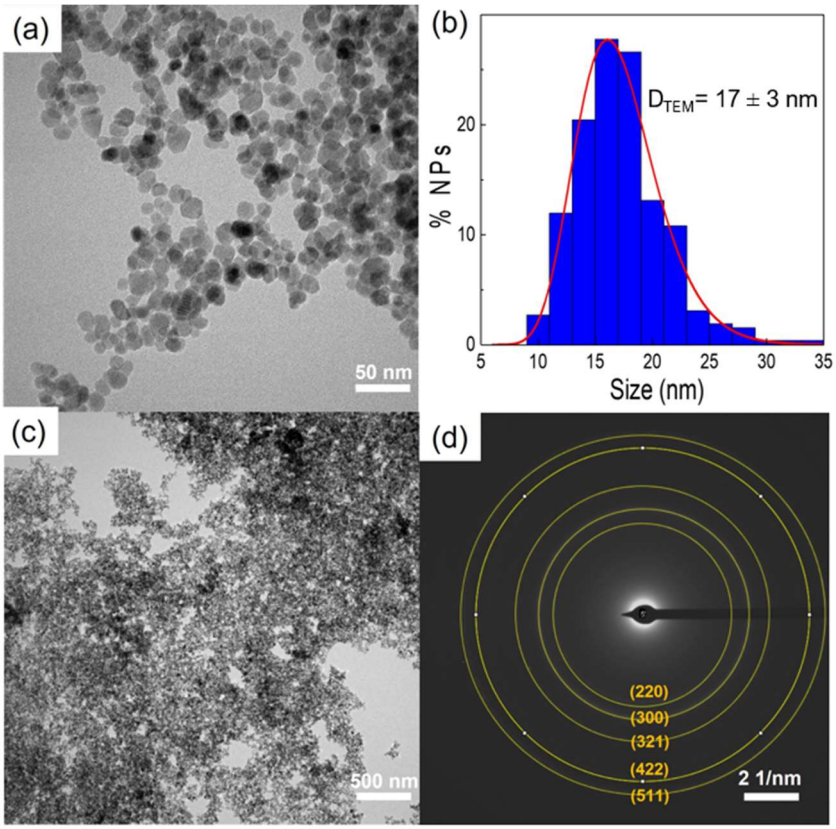

Figure S4. TEM characterization for the sample IONPs@X4C4. (a) High magnification TEM image (scale bare of 50 nm). (b) Particle size distribution with an average size of 17 ± 3 nm. (c) Low magnification TEM image (scale bar of 500 nm) and its corresponding SAED characterization showing the intense pattern rings of the γ-Fe_2O_3 phase.

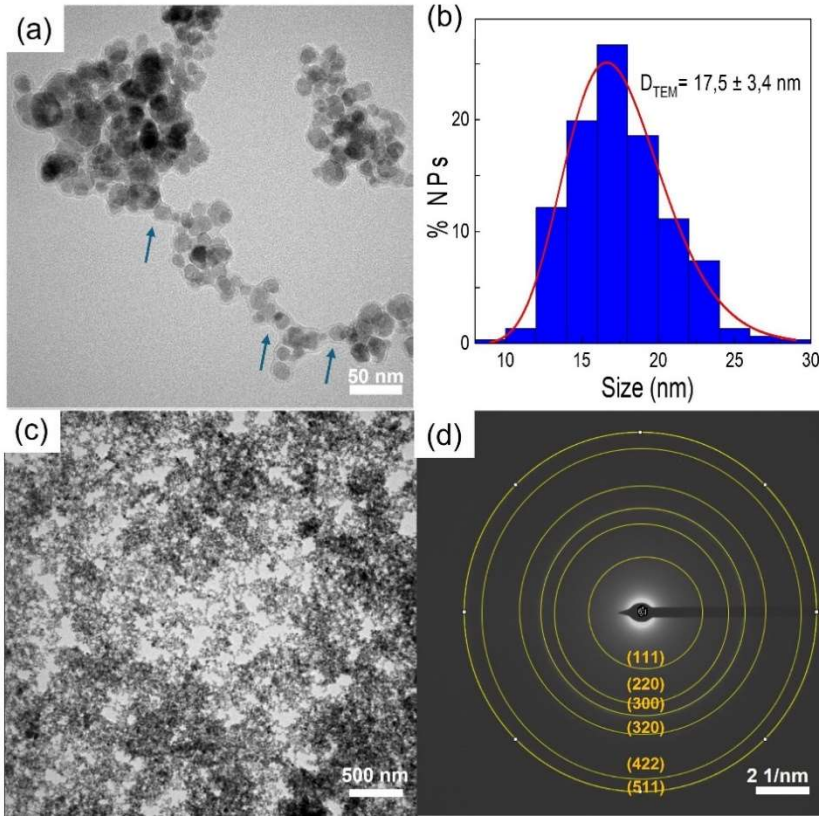

Figure S5. TEM characterization for the sample IONPs@X4C4@PEI. (a) High magnification TEM image (scale bare of 50 nm). (b) Particle size distribution with an average size of 18 ± 3 nm. (c) Low magnification TEM image (scale bar of 500 nm) and its corresponding SAED characterization showing the intense pattern rings of the γ-Fe_2O_3 phase.

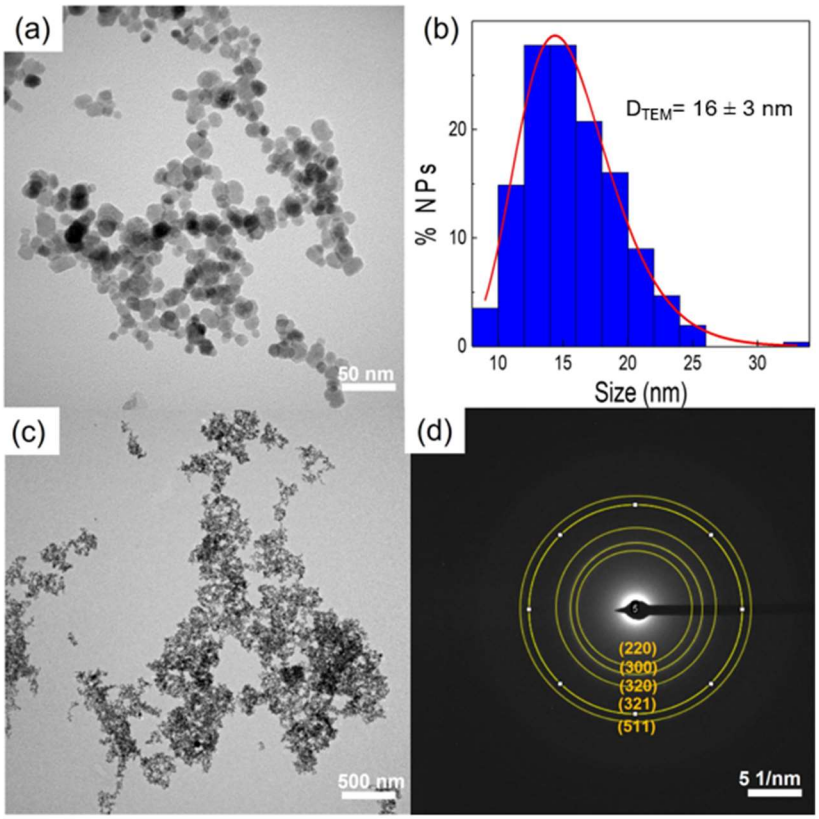

Figure S6. TEM characterization for the sample IONPs@XC. (a) High magnification TEM image (scale bare of 50 nm). (b) Particle size distribution with an average size of 16 ± 3 nm. (c) Low magnification TEM image (scale bar of 500 nm) and its corresponding SAED characterization showing the intense pattern rings of the γ-Fe_2O_3 phase.

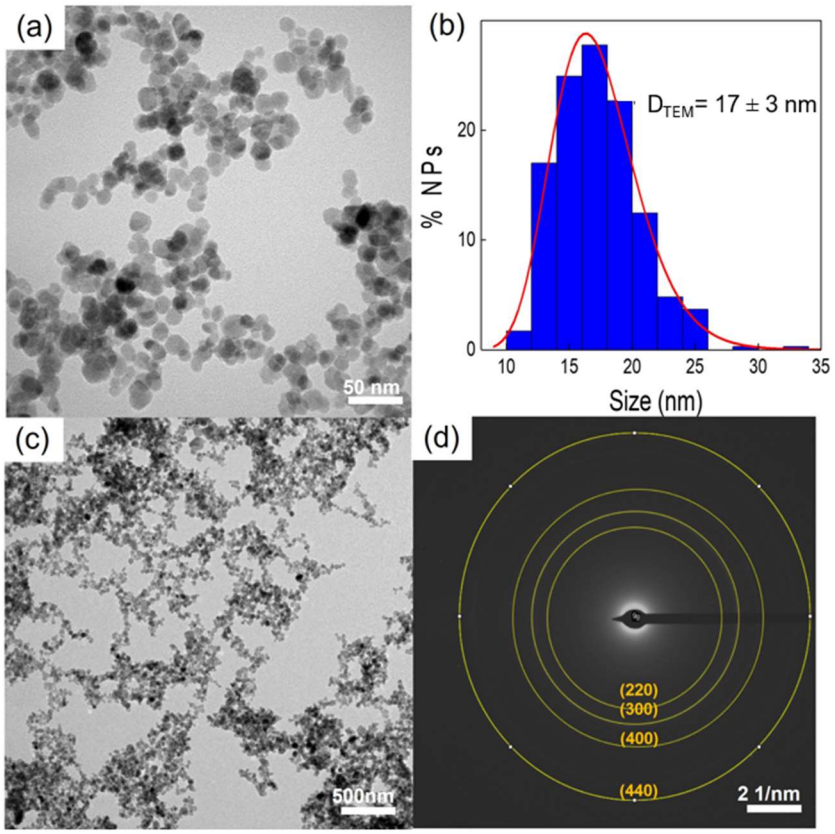

Figure S7. TEM characterization for the sample IONPs@XC@PEI. (a) High magnification TEM image (scale bare of 50 nm). (b) Particle size distribution with an average size of 17 ± 3 nm. (c) Low magnification TEM image (scale bar of 500 nm) and its corresponding SAED characterization showing the more intense pattern rings of the γ-Fe_2O_3 phase

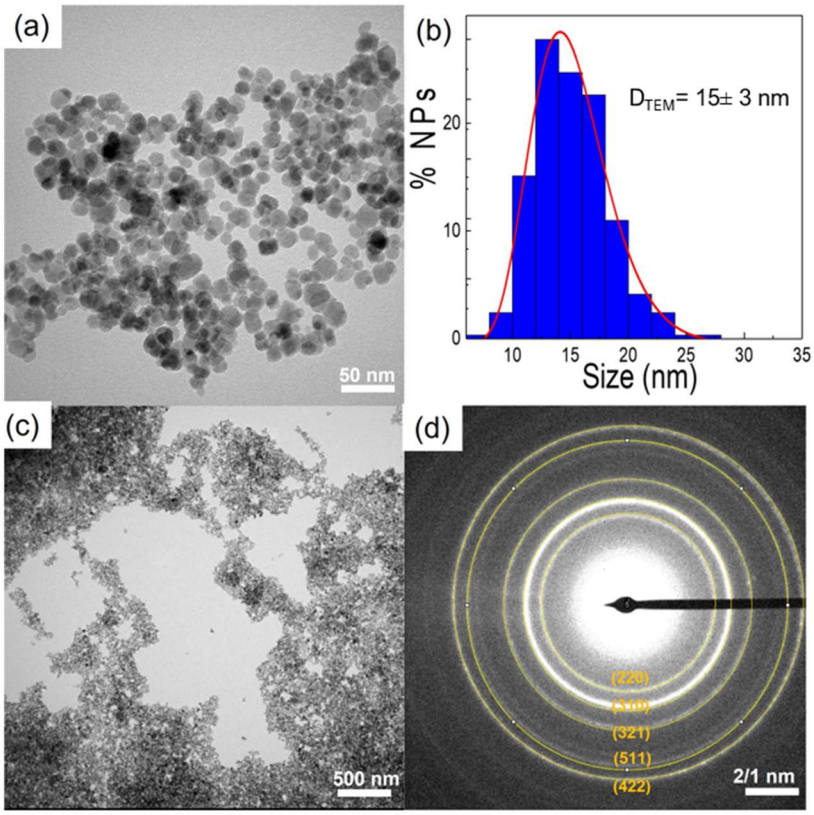

Figure S8. TEM characterization for the sample IONPs@Cit. (a) High magnification TEM image (scale bare of 50 nm). (b) Particle size distribution with an average size of 15 ± 3 nm. (c) Low magnification TEM image (scale bar of 500 nm) and its corresponding SAED characterization showing the more intense pattern rings of the γ-Fe_2O_3 phase.

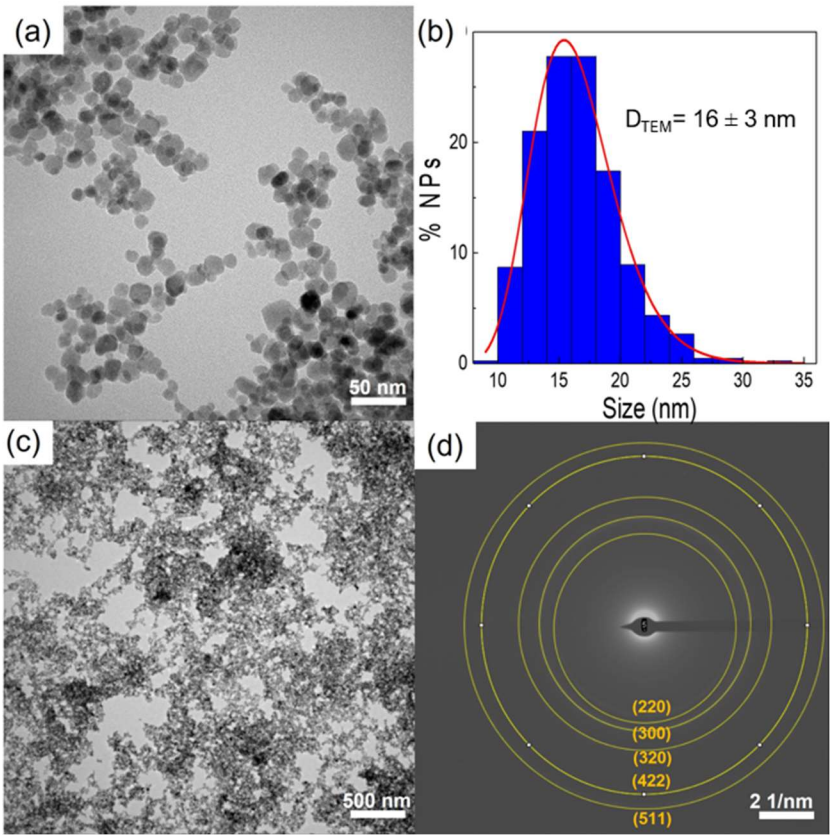

Figure S9. TEM characterization for the sample IONPs@Cit@PEI. (a) High magnification TEM image (scale bare of 50 nm). (b) Particle size distribution with an average size of 16 ± 3 nm. (c) Low magnification TEM image (scale bar of 500 nm) and its corresponding SAED characterization showing the more intense pattern rings of the γ-Fe_2O_3 phase.

.

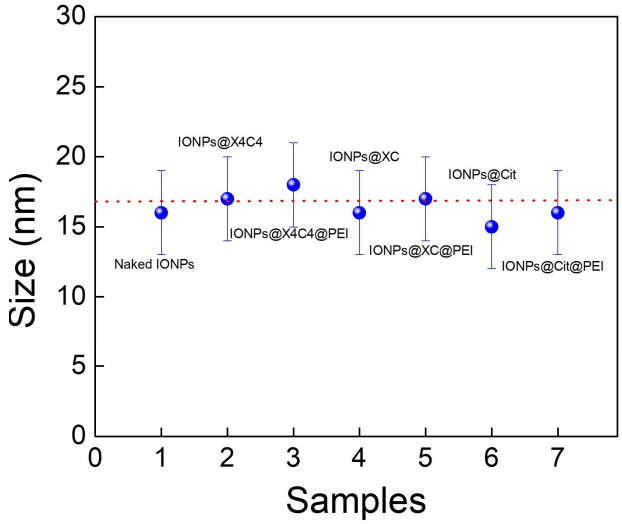

Figure S10. Graphical comparison of the D_{TEM} of the different batches of IONPs. The dotted line is centered on the average $D_{TEM} = 16.4$ nm of all the samples.

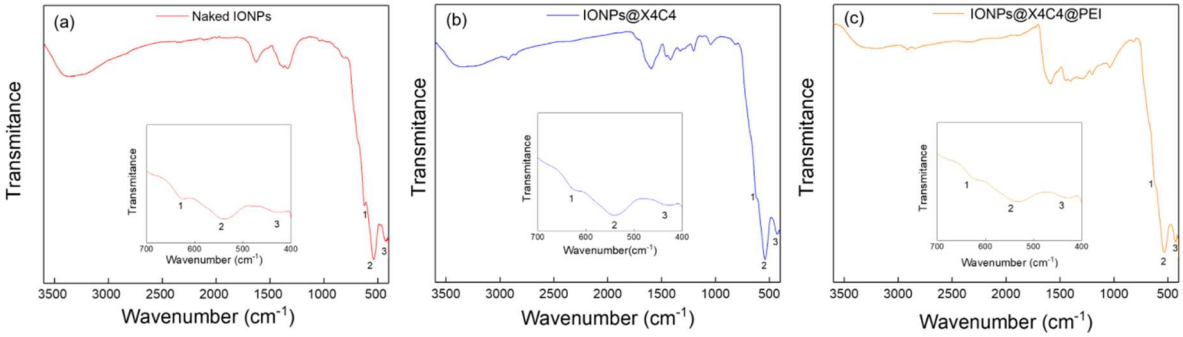

Figure S11. FTIR spectra of (a) naked IONPs, (b) IONPs@X4C4, and (c) IONPs@X4C4@PEI analyzed using a Thermo SCIENTIFIC NICOLET iZ10 infrared spectrometer, with measurements conducted over a spectral range of 400 to 4000 cm^{-1} at a resolution of 1 cm^{-1}. The insets show the FTIR spectra at lower wavenumber, focusing on the main absorption bands corresponding to the Fe–O stretching vibrations, labeled as 1, 2, and 3.

Table S3. FTIR peak positions for naked IONPs, IONPs@X4C4, and IONPs@X4C4@PEI, compared to the reference peaks for γ-Fe_2O_3 and Fe_3O_4.[2]

	peak 1 (cm^{-1})	peak 2 (cm^{-1})	peak 3 (cm^{-1})
naked IONPs	626	537	430
IONPs@X4C4	626	540	430
IONPs@X4C4@PEI	627	535	428
γ-Fe_2O_3	630	590	430
Fe_3O_4	570		390

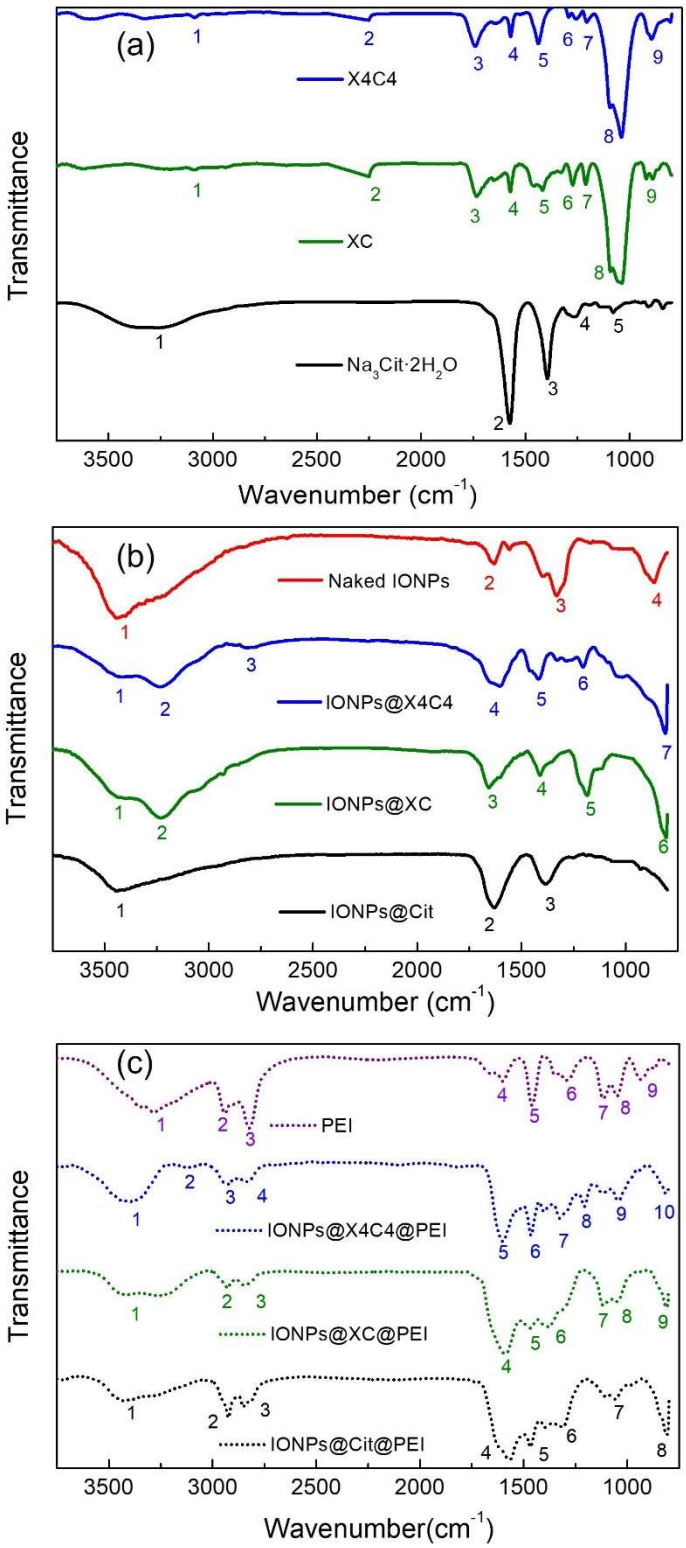

Figure S12 . FTIR spectra from 3750 to 750 cm^{-1} for (a) the organic coating molecules used in this work. X4C4-tera-diazonium, XC-diazonium, and $Na_3Cit \cdot 2H_2O$. (b) FTIR spectra for the IONPs@X4C4, IONPs@XC, and IONPs@Cit samples. (c) FTIR spectra of the PEI functionalized series of samples and their comparison with that of the PEI polymer.

Table S4. Main FTIR bands corresponding to Figure S10.(a) Functionalization agents X4C4-tetra-diazonium, XC-diazonium, and Cit employed for the functionalization of IONPs. (b) Functionalized IONPs@X4C4, IONPs@XC, and IONPs@Cit samples. (c) PEI coated functionalized IONP samples.

(a)

X4C4-tetra-diazonium	Band (cm^{-1})	Functional group
1	3084	C-H st
2	2253	N-N st
3	1740	C=O st ($RCOO^-$)
4	1566	Asy COO^- st
5	1422	Sy COO^- st
6	1274	C-O st (phenoxy)
7	1182	C-O st (aromatic)
8	1033	C-O st (ether)
9	889	C-H bend (aromatic)
XC-diazonium	**Band (cm^{-1})**	**Functional group**
1	3084	C-H st
2	2258	N-N st
3	1730	C=O st ($RCOO^-$)
4	1570	Asy COO^- st
5	1427	Sy COO^- st
6	1273	C-O st (phenoxy)
7	1187	C-O st (aromatic)
8	1048	C-O st (ether)
9	909	C-H bend (aromatic)
$Na_3Cit \cdot 2H_2O$	**Band (cm^{-1})**	**Functional group**
1	3289	O-H st
2	1566	Asy COO^- st
3	1381	Sy COO^- st
4	1253	C-O st (COO-)
5	1069	C-O-C st

(b)

Naked IONPs	Band (cm^{-1})	Functional group
1	3443	O-H st
2	1643	O-H ben (H_2O)
3	1325	Asy N-O (NO_3^-)
4	851	O-H ben (out of plane)
IONPs@X4C4	**Band (cm^{-1})**	**Functional group**
1	3396	O-H st
2	3227	O-H st (sec)
3	2843	C-H st
4	1616	Asy COO^- st
5	1416	Sy COO^- st
6	1211	C-O st (ether)
7	811	C-H bend (aromatic)
IONPs@XC	**Band (cm^{-1})**	**Functional group**
1	3421	O-H st
2	3211	O-H st (sec)
3	1658	Asy COO^- st
4	1391	Sy COO^- st
5	1181	C-O st (ether)
6	802	C-H bend (aromatic)
IONPs@Cit	**Band (cm^{-1})**	**Functional group**
1	3442	O-H st
2	1622	Asy COO^- st
3	1386	Sy COO^- st

(c)

PEI	Band (cm^{-1})	Functional group
1	3278	N-H st
2	2950	Asy C-H st
3	2817	Sy C-H st
4	1607	N-H ben
5	1458	C-H ben
6	1284	C-N st (sec.amine)
7	1110	C-N st (constrain)
8	1037	C-N st (prim.amine)
9	930	N-H wag
IONPs@X4C4@PEI	**Band (cm^{-1})**	**Functional group**
1	3411	O-H st
2	3119	C-H st (aliphatic)
3	2924	Asy C-H st
4	2806	Sy C-H st
5	1607	N-H ben
6	1453	C-H ben
7	1325	Sy COO^- st
8	1202	C-N st (sec.amine)
9	1028	C-N st (prim.amine)
10	812	C-H bend (aromatic)
IONPs@XC@PEI	**Band (cm^{-1})**	**Functional group**
1	3432	O-H st
2	3243	C-H st (aliphatic)
3	2919	Asy C-H st
4	2821	Sy C-H st
5	1586	N-H ben
6	1463	C-H ben
7	1381	Sy COO^- st
8	1110	C-N st (constrain)
9	1028	C-N st (prim.amine)
10	812	C-H bend (aromatic)
IONPs@Cit@PEI	**Band (cm^{-1})**	**Functional group**
1	3416	O-H st
2	2919	Asy C-H st
3	2837	Sy C-H st
4	1566	N-H ben
5	1453	C-H ben
6	1320	Sy COO^- st
7	1048	C-N st (prim.amine)
8	802	C-H bend (aromatic)

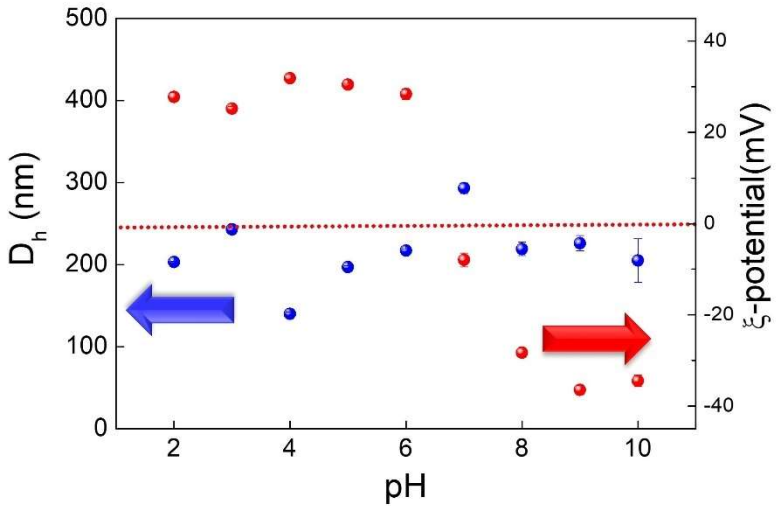

Figure S13. Correlation of D_h, (blue dots) and ζ-potential (red dots) of the naked IONPs from pH 2 to 10 in MQ-H_2O. The blue dots represent D_h measured in nanometers (nm), with the scale on the left indicated by the blue arrow, while the red dots denote ζ-potential in millivolts (mV), with the scale on the right highlighted by the red arrow.

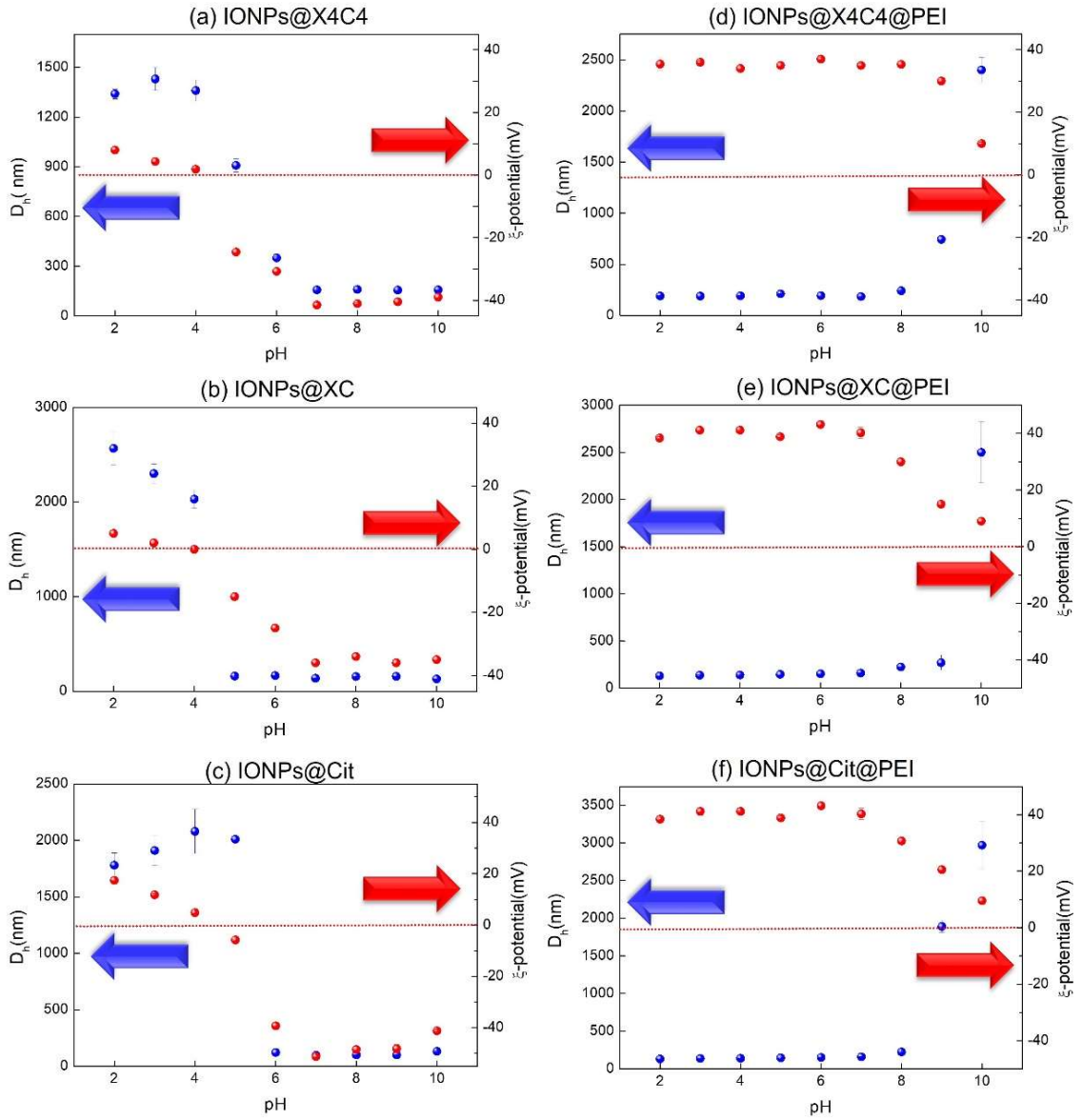

Figure S14. pH-dependent D_h, (blue dots) and ζ-potential (red dots) for the functionalized IONPs synthesized in this work from pH 2 to 10 in MQ-H_2O. The left-side panel shows the behavior of the (a) IONPs@X4C4, (b) IONPs@XC, and (c) IONPs@Cit samples. The right-side panel shows the pH dependence of these two parameters for the PEI-coated IONPs. (d) IONPs@X4C4@PEI, (e) IONPs@XC@PEI, and (f) IONPs@Cit@PEI samples.

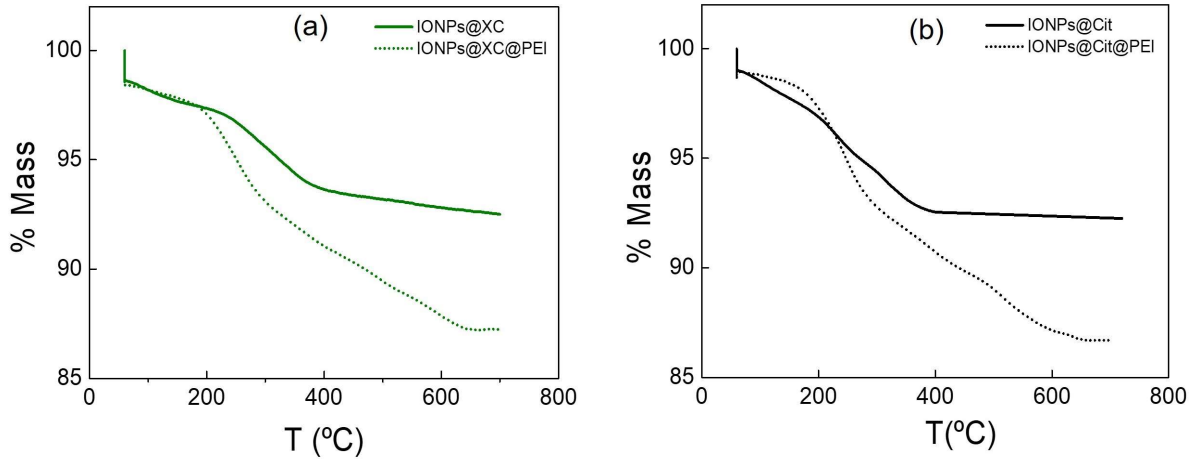

Figure S15. TGA curves of the (a) IONPs@XC, and IONPs@XC@PEI, and (b) IONPs@Cit, and IONPs@Cit@PEI samples.

Table S5. Quantitative Analysis of TGA results for the functionalized samples. Calculations were done assuming spherical shape IONPs according to the D_{TEM}. IONP's Volume (V) and Surface Area (S) derived from $V = 4/3\ \pi R^3$ and $S = 4\pi R^2$ equations, respectively. Where R stands for the IONP's radius.

Functionalization agent	**X4C4**	**PEI (X4C4@PEI)**	**XC**	**PEI (XC@PEI)**	**Cit**	**PEI (Cit@PEI)**
% Organic fraction	14	9	6	5	6	5
MW (g/mol)	664	25000	152.14	25000	189.1	25000
$D_{TEM} \pm \sigma$ (nm)	17 ± 3	18 ± 3	16 ± 3	17 ± 3	15 ± 3	18 ± 3
Density γ-Fe_2O_3 (g/cm^3)	4.9	4.9	4.9	4.9	4.9	4.9
Volume of IONP (nm^3)	2572	3054	2145	2572	1767	3054
Nº molecules	6.35E+19	8.43E+17	1.19E+20	6.02E+17	9.56E+19	6.02E+17
Nº IONPs	3.37E+16	2.57E+16	4.38E+16	3.49E+16	5.31E+16	3.49E+16
S (nm^2) IONP	908	1018	804	908	707	1018
(Organic molecules/IONP) ± σ	1883 ± 733	33 ± 12	2684 ± 1254	17 ± 8	1779± 798	17 ± 7
(Organic molecule/nm^2) ± σ	2.1 ± 0.3	0.04±0.01	3.3 ± 0.9	0.02±0.01	2.5 ± 0.6	0.02±0.01

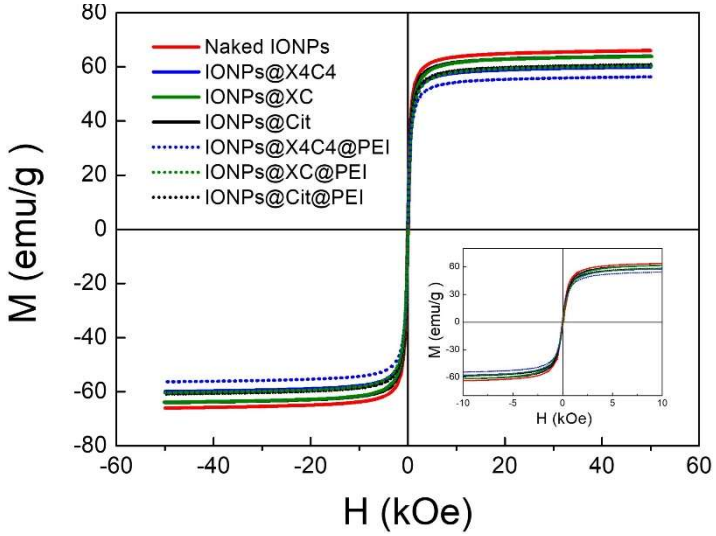

Figure S16. Hysteresis loops at room temperature with a maximum field of H= ± 50 kOe for the series of IONPs prepared and functionalized in this work. Naked IONPs (red plain line), IONPs@X4C4 (blue plain line), IONPs@XC (green plain line), IONPs@Cit (black plain line), IONPs@X4C4@PEI (blue dotted line), IONPs@XC@PEI (green dotted line), and IONPs@Cit@PEI (black dotted line).

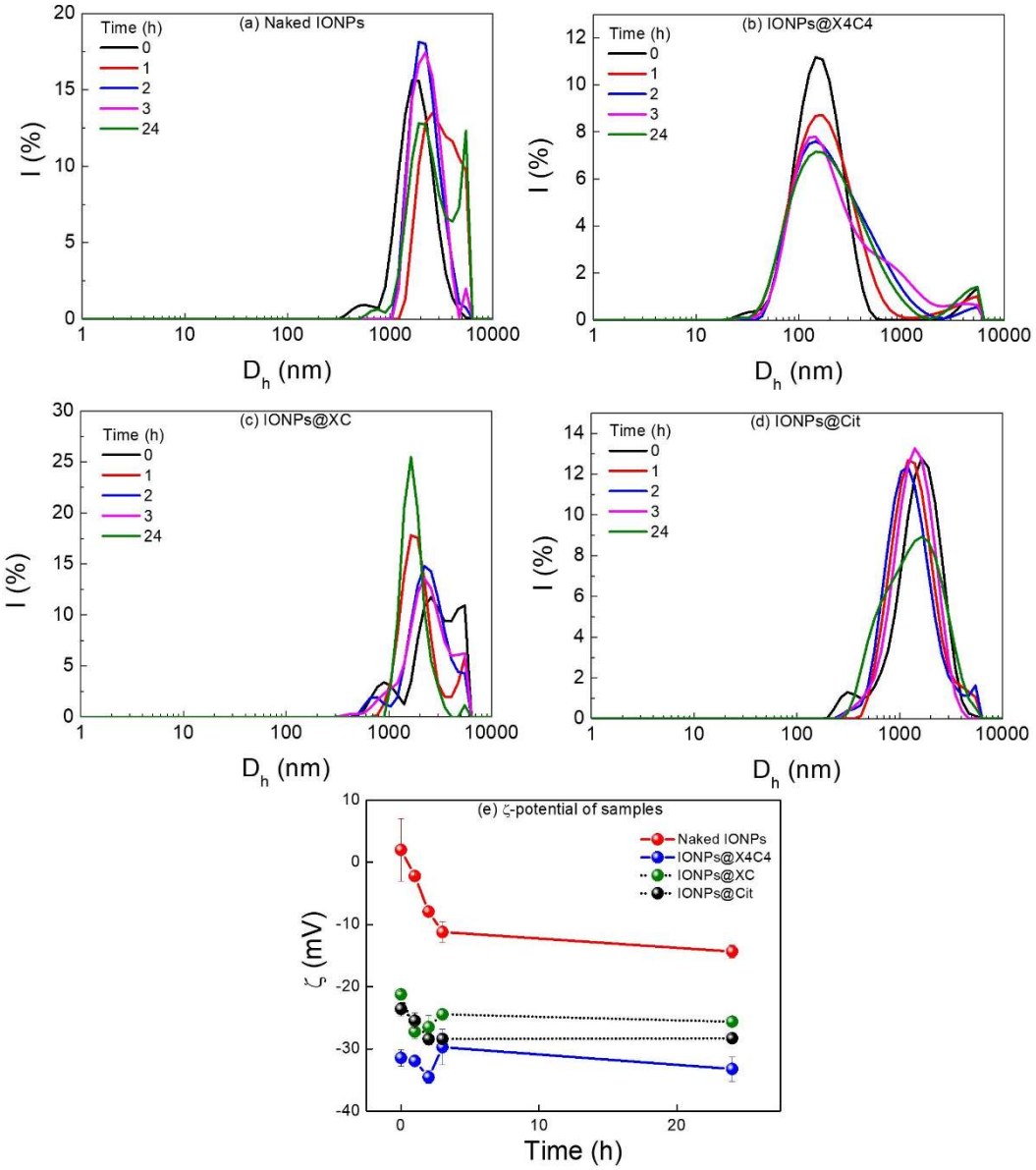

Figure S17. Comparative analysis of particle stability in 0.1 M NaCl at pH 7. DLS evolution of (a) naked IONPs, (b) IONPs@X4C4, (c) IONPs@XC, and (d) IONPs@Cit samples for the following incubation times: 0, 1, 2, 3, and 24h.
(e) Evolution of the ζ-potential of the samples over 24h in 0.1 M NaCl at pH 7.

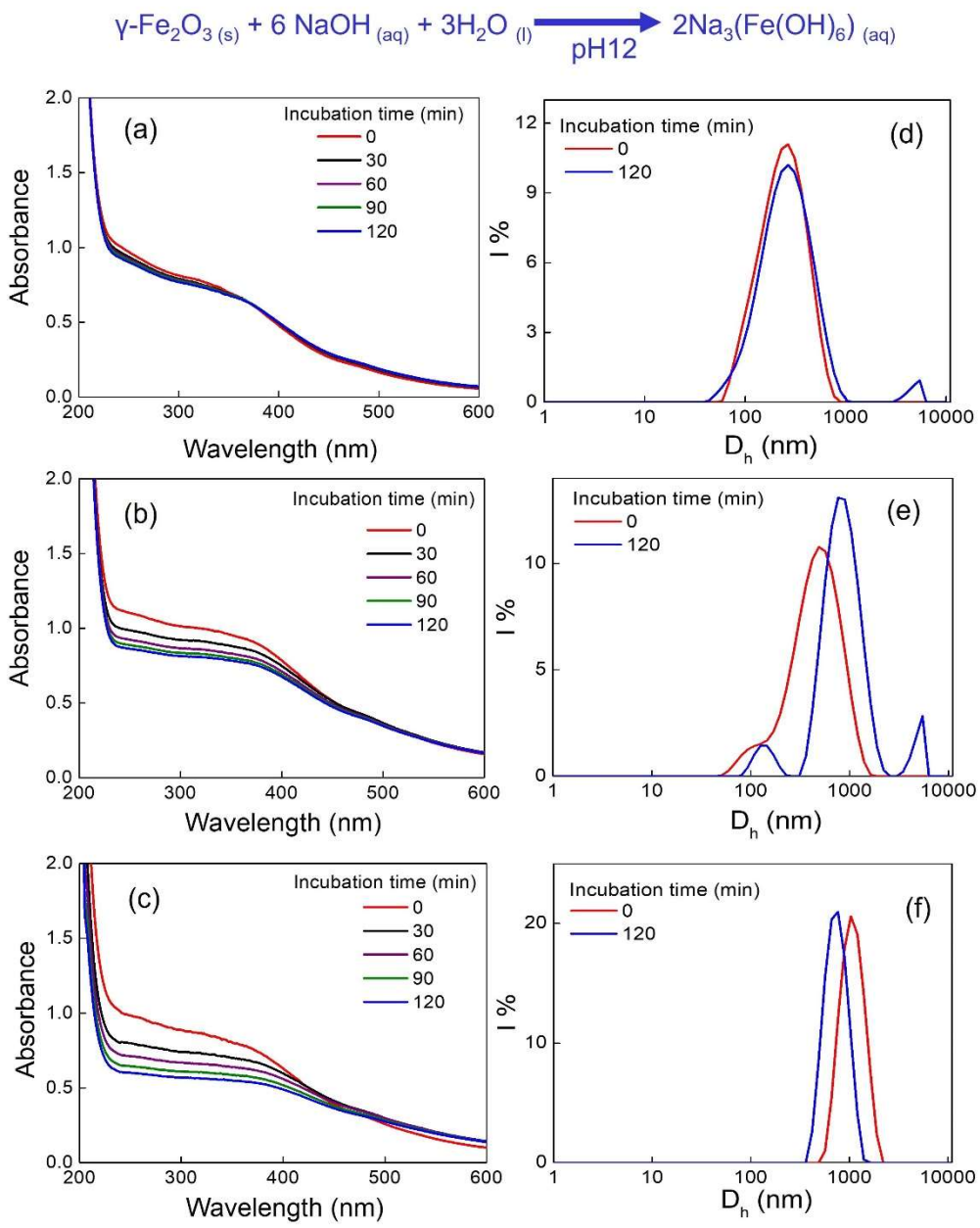

Figure S18. Monitoring of the IONP core digestion at pH 12 of the functionalized IONPs. UV-Vis absorption spectra as a function of time of (a) IONPs@X4C4, (b) IONPs@XC, and (c) IONPs@Cit samples. DLS curves at 0 and after 120 min of incubation at pH12 of the functionalized IONPs. (d) IONPs@X4C4, (e) IONPs@XC, and (f) IONPs@Cit samples.

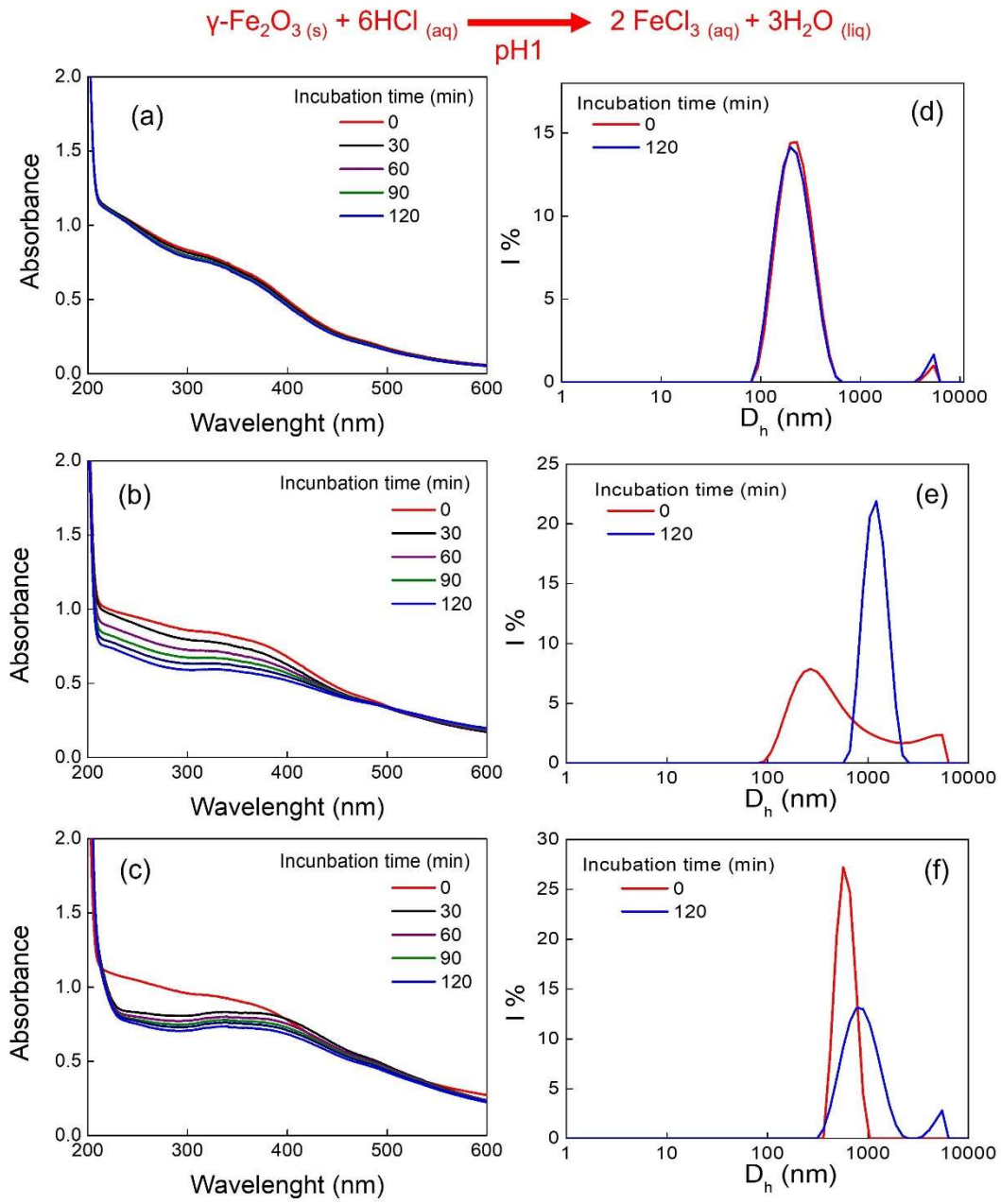

Figure S19. Monitoring of the IONP core digestion at pH 1 of the functionalized IONPs. UV-Vis absorption spectra as a function of time of (a) IONPs@X4C4@PEI, (b) IONPs@XC@PEI, and (c) IONPs@Cit@PEI samples. DLS curves at 0 and after 120 min of incubation at pH1 of the functionalized IONPs. (d) IONPs@X4C4@PEI, (e) IONPs@XC@PEI, and (f) IONPs@Cit@PEI samples.

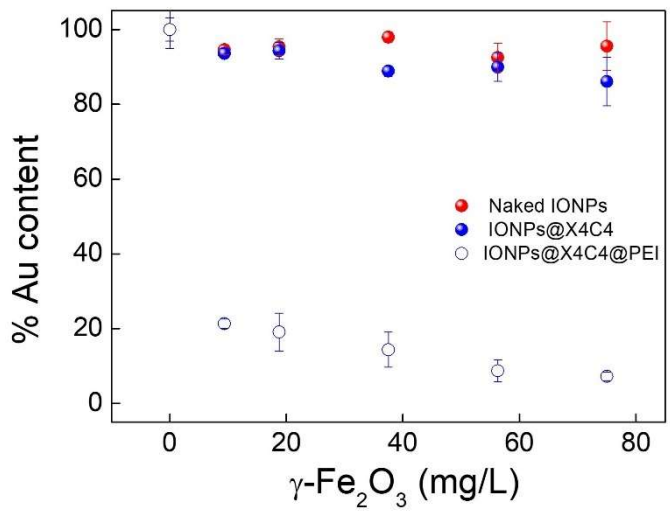

Figure S20. Comparison of Au remaining in the supernatant at pH8 after collection experiments with naked IONPs (red solid spheres), IONPs@X4C4 (blue solid spheres), and IONPs@X4C4@PEI (blue empty spheres) as a function of the total amount of particles (quantified as the weight of γ-Fe_2O_3 added) added.

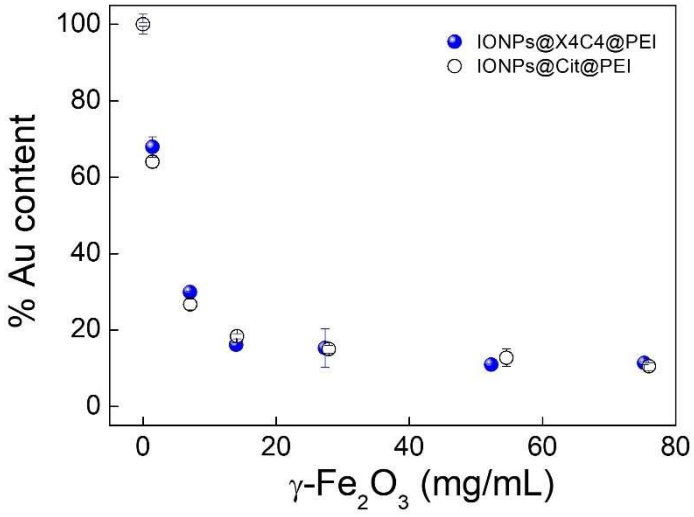

Figure S21. Comparison of Au remaining in the supernatant at pH8 after collection experiments with IONPs@X4C4@PEI (blue solid spheres) and IONPs@Cit@PEI (black empty spheres) samples as a function of the total amount of particles (quantified as the weight of γ-Fe_2O_3 added) added.

Table S6. Comparison of various IONP systems for the extraction of Au^{3+} ions from different aqueous environments. The table summarizes the type of particles used, their gold adsorption capacities (Q, in mAu^{3+}/gIONP), experimental conditions, Au^{3+} concentration, release methodology, and references.

Work	Type of particle	Q ($mgAu^{3+}$)/gIONP)	Conditions	Au^{3+} concentration (mg/L)	Release methodology / % release	Reference
1	Naked IONPs	2.3	pH 6.5, NaCl concentration varied from 0.1 M to 3.0 M, incubation of 24h	10-100	Not described	3
2	IONPs@squamides	Not described	pH 2, $AuCl_4$, 25°C, reduction of Au, 2h of incubation	5	Not described	4
3	IONPs@Cit@PEI	42.5	pH 8, 0.1 M thiosulfate, 25°C, from 1-24h of incubation	10	Addition of 0.01 M NaOH up to pH 12. Magnetic separation and gold collection from the supernatant. Nearly 100% released	5
This work	**IONPs@X4C4@PEI**	**12.6**	**pH 8, 25°C, from 0 to 1h**	**0.076**	**Addition of thiourea at pH 3. Magnetic separation and gold collection from the supernatant. Nearly 100% released**	
This work	**IONPs@Cit@PEI**	**12.8**	**pH 8, 25°C, from 0 to 1h**	**0.076**	**Addition of thiourea at pH 3. Magnetic separation and gold collection from the supernatant. Nearly 100% released**	
5	Chitosan resine embeding IONPs	709.2	pH 0.5, incubation times from 0.15 to 2h	2364	Addition of 0.5 M thiourea acidified with 0.2 M H_2SO_4. Flow rate of 1 mL/min and thorough washing for reuse. Nearly 100% released	6
6	IONPs@Moringa proteins	107	2h at pH 2.5	10	Not described	7
7	$CoFe_2O_4$@MPTS	120	pH from 1to 4	10	Addition of 1 M thiourea in 1 M HCl. 85% released	8
8	IONPs modified with dendrimer and palmitic acid	6.5-8.3	pH 3, 25ºC	9.78	Desorption using 1 M HNO_3, 0.5 M thiourea. 55% released	9
9	IONPs-SiO_2-thiol	84.75	pH 5, 30°C, 4 h	20	1 mol/L HCl containing 2% thiourea. 96.2% released	10
10	IONPs-thiourea	118.5	pH 2, 25ºC, 0.5h	50 to 110	0.7 M thiourea and 2% HCl. Nearly 100% released	11

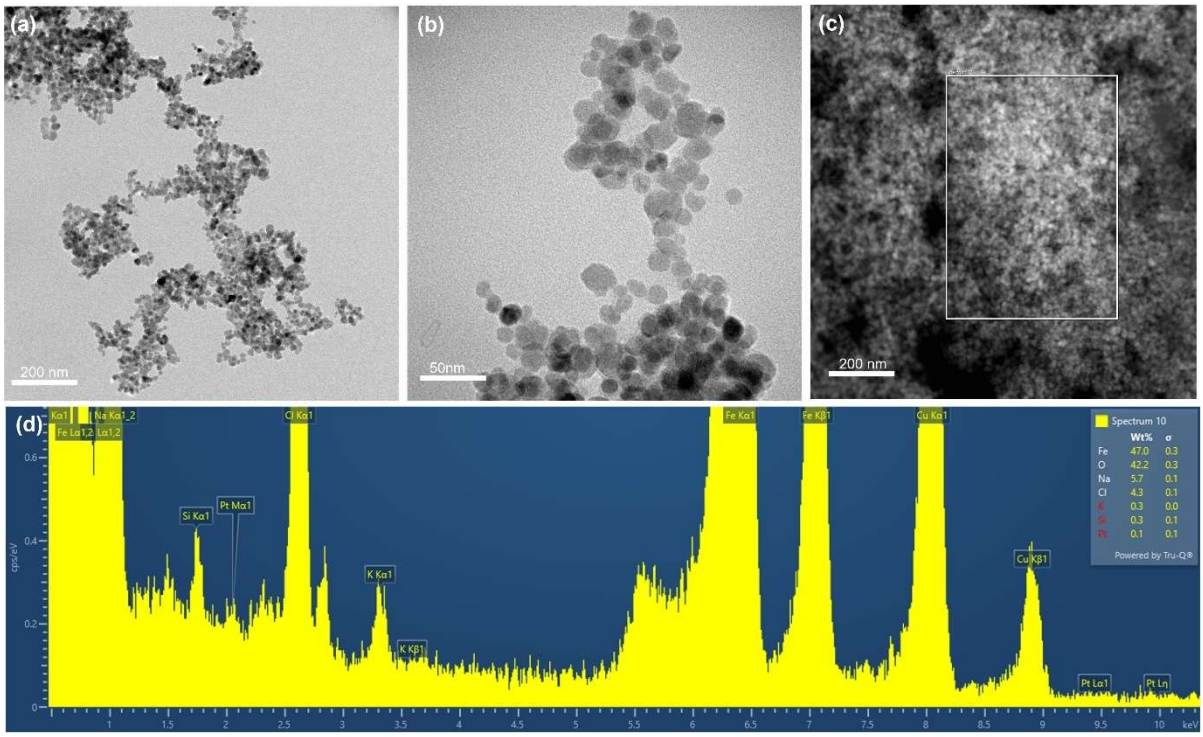

Figure S22. Gallery of TEM images showing IONPs@X4C4@PEI after one collection process in a synthetic Pt chloride solution. From (a) to (b) : bright field TEM images at several magnifications of IONPs@X4C4@PEI particles. (c) HAADF-STEM image correlated with (d) an EDS spectrum analysis for elemental composition determination.

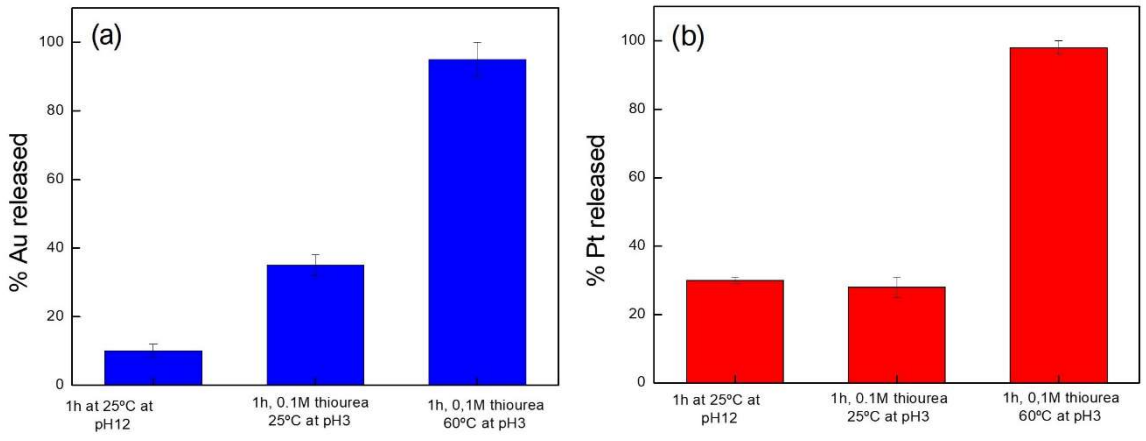

Figure S23. (a) Au(III) and (b) Pt(IV) released from the IONPs@X4C4@PEI under three different conditions.

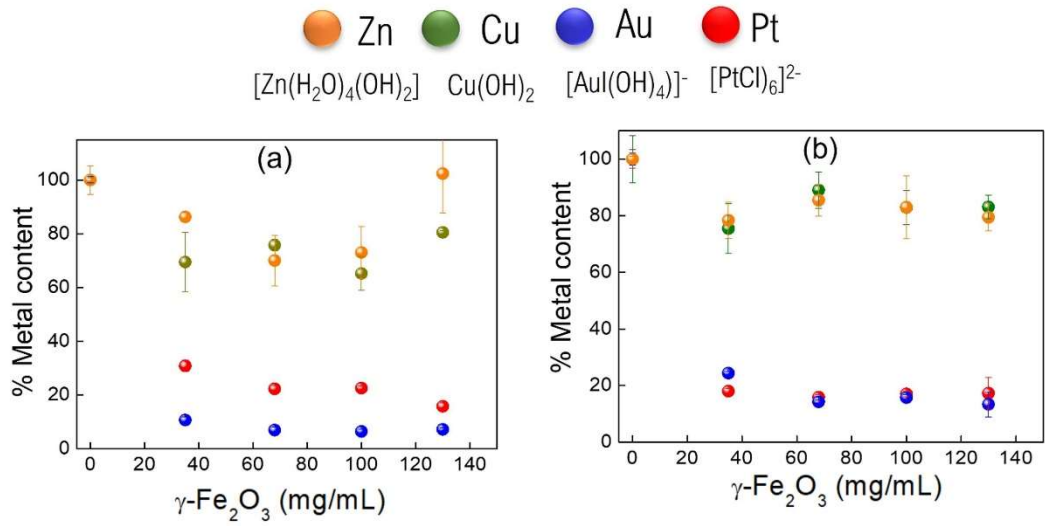

Figure S24. Percentage of the initial metal concentration remaining in supernatant after extraction experiments at 25°C (left) and 50°C (right) for a mixture of metals containing [Zn] = [Cu] = 3x[Au, Pt] and [Au] equal to 76 µg/L.

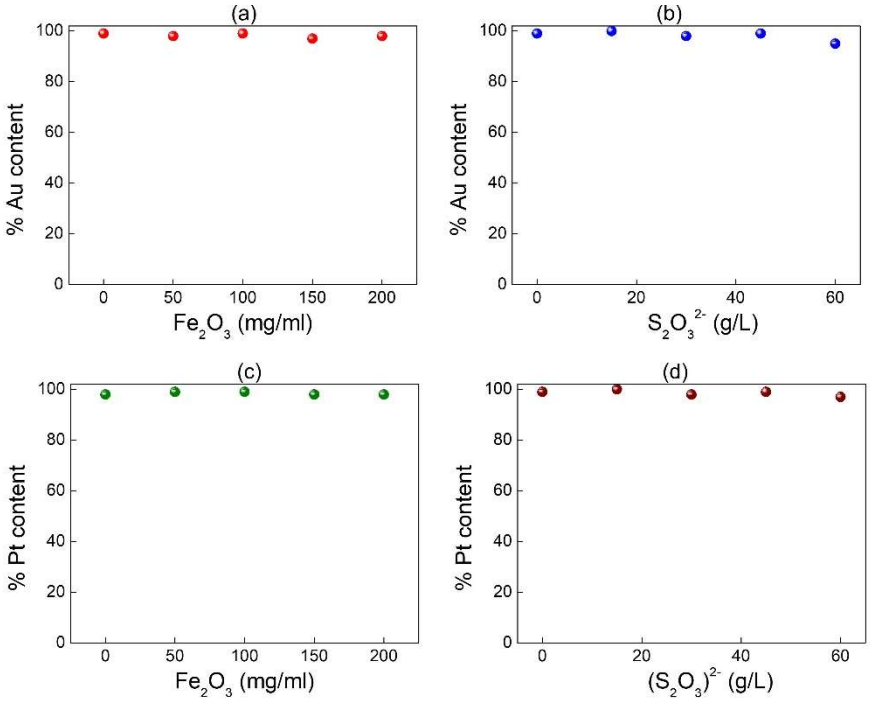

Figure S25. Collection capacity of the IONPs@X4C4@PEI sample in WetOX after 12 hours of incubation at 50°C under various conditions. (a) and (c) show the % Au and % Pt content, respectively, when using increasing concentrations of IONPs, ranging from 0 to 184 mg Fe_2O_3/ml. (b) and (d) display the % Au and % Pt content, respectively, after incubating the particles with an 184 mg Fe_2O_3/ml concentration and increasing amounts of $(S_2O_3)^{2-}$.

References

1. Torras, M.; Moya, C.; Pasquevich, G. A.; Roig, A. Accurate Iron Quantification in Colloids and Nanocomposites by a Simple UV-Vis Protocol. *Microchim. Acta* **2020**, *187* (9), 488-498.

2. S. P. Schwaminger, D. Bauer, P. Fraga-García, F. E. Wagner and S. Berensmeier, *CrystEngComm*, **2017**, 19, 246-255.

3. A.R.M. Calderon, R.D. Alorro, B. Tadesse, K. Yoo and C.B. Tabelin, *JOM*, **2019**, 71, 4183-4191.

4. P. Duel, M. S. Gutiérrez, P. Rodríguez, A. León, K. A. López, J. Morey and M. N. Piña, *RSC Adv.*, **2018**, 8, 36123 -36132.

5. N.D. Ilankoon, C. Aldrich, E.A. Oraby and J.J. Eksteen, *Hydrometallurgy*, **2020**, 195, 105375.

6. A.M. Donia, A.A. Atia and K.Z. Elwakeel, *Hydrometallurgy*, **2007**, 87, 197-206.

7. M.O.N. Amuanyena, M. Kandawa-Schulz and H.M. Kwaambwa, *J. Biomater. Nanobiotechnol.*, **2019**, 10, 142-158.

8. A. Kraus, K. Jainae, F. Unob and N. Sukpirom, *J. Colloid Interface Sci.*, **2009**, 338, 359-365.

9. J. T. Khutlane, K. R. Koch and R. Malgas-Enus, *SN Appl. Sci.*, **2020**, 2, 1125.

10. Y. Zhang, Q. Xu, S. Zhang, J. Liu, J. Zhou, H. Xu, H. Xiao and J. Li, *Sep. Purif. Technol.*, **2013**, 116, 391-397.

11. Tai-Lin Lin and Hsing-Lung Lien, *Int. J. Mol. Sci.*, **2013**, 14, 9834-9847.